Surface & Coatings Technology 205 (2011) 4934–4940

Contents lists available at ScienceDirect

Surface & Coatings Technology

journal homepage: www.elsevier.com/locate/surfcoat

On the use of radioisotopes to study the possible synthesis by magnetron sputtering of bimetallic nanoparticles

V. Bouchat [a,h], N. Moreau [a,h], V. Valembois [a,h], K. Abbas [b], O. Feron [c], B. Gallez [d], U. Holzwarth [b], B. Masereel [e,h], C. Michiels [f,h], F. Simonelli [b], T. Vander Borght [g,h], S. Lucas [a,h,*]

[a] Research Center for the Physics of Matter and Radiation (PMR), Laboratoire d'Analyses par Réactions Nucléaires (LARN), FUNDP University of Namur, Namur, Belgium
[b] Institute for Health and Consumer Protection, Joint Research Centre (JRC), European Commission, Ispra, Italy
[c] Unité de Pharmacothérapie (FATH), Université catholique de Louvain, Brussels, Belgium
[d] Laboratoire de résonance magnétique biomédicale (CMFA), Université catholique de Louvain, Brussels, Belgium
[e] Département de Pharmacie (DP), FUNDP University of Namur, Namur, Belgium
[f] Unité de Recherche en Biologie Cellulaire (URBC), FUNDP University of Namur, Namur, Belgium
[g] Center for Molecular Imaging and Experimental Radiotherapy (IRME), Université catholique de Louvain, Yvoir, Belgium
[h] NARILIS – Namur Research Institute for Life Sciences, Namur, Belgium

ARTICLE INFO

Article history:
Received 16 February 2011
Accepted in revised form 19 April 2011
Available online 27 April 2011

Keywords:
Magnetron discharges
Nanoparticles
Radioisotopes

ABSTRACT

An approach using physical vapor deposition technology to produce nanoparticles (NPs) containing radioactive atoms and the methodology to transfer them in pure water is investigated. NPs are synthesized by magnetron sputtering at high pressure and radioactive atoms are loaded on magnetron cathodes prior to sputtering. The technique was tested for gold cathode loaded with $^{57/58}$Co and $^{195/196}$Au. Linked to biological vector molecules, the nanoparticles can be used to enhance diagnostic sensitivity in medical imaging or to treat cancer.

Sizes and morphologies of the NPs were analyzed by electron microscopy, UV-Visible spectroscopy and atomic absorption spectroscopy. Results show well dispersed NPs with sizes varying between 5 and 10 nm. Activities of these NPs were measured with a CAPINTEC well counter and a High Purity Germanium detector system. Centrifugation analyses also demonstrate that the choice of the activated metal which can be alloyed with NPs plays an important role in the synthesis. This was confirmed by the Au–Co phase diagram that shows that cobalt cannot be included efficiently in the gold NPs conversely to gold.

© 2011 Elsevier B.V. All rights reserved.

1. Introduction

We recently investigated the possibility to synthesize sub 10 nm NPs by magnetron sputtering. This technique, based on aggregation and growth in gas phase can be used to produce non-agglomerated metallic NPs with a narrow size distribution [1–5].

The technique was proposed for the first time by Takagi in 1972 to produce high quality films by ionized cluster beam (ICB) deposition [3]. Their idea was to generate a cluster beam formed by inert gas condensation (IGC) after evaporation of film materials. A few years later, Haberland et al. decided to vaporize the film material by magnetron sputtering rather than by evaporation [6]. Magnetron sputtering has the advantage to produce atomic vapor from a wide variety of solid materials or composites. Sputtering allows for the deposition of films having the same composition as target source, and when used in co-sputtering mode, one can vary the coating concentration over a large range.

In this study, we investigated the possibility to synthesize sub-10 nm Au–Co nanoparticles with a large amount of Co by magnetron sputtering. One special feature of the work is that we used radioactive Co and Au as a main investigation tool to control and to assess the production yield of NPs.

This method using radioactivity as a tool for detection is far more straightforward with respect to the traditional ones such as XPS or EDX (Energy Dispersive X-ray Analyis).

The strategy involved the synthesis and immobilization of NPs on a soluble substrate (NaCl) that is later dissolved in water. Activity evaluation of the solution and the NPs were performed after centrifugation by measuring the amount of radiation emitted either by the supernatant or the solid phase. By doing so, it is possible to evaluate if Co atoms are mixed with those of Au in the solid NPs and to examine if bulk phase diagrams of bimetallic materials are still valid for NPs as a large fraction of atoms resides on the surfaces [7]. For example, surface segregation of bimetallic NPs has already been observed in which chemical composition at surface differs from that in bulk [8–11]. Therefore, the properties of miscibility of individual

* Corresponding author at: Research Centre for the Physics of Matter and Radiation (PMR-LARN), University of Namur (FUNDP), 61 Rue de Bruxelles, B-5000 Namur, Belgium. Tel.: +32 81 72 54 81; fax: +32 81 72 54 74.
E-mail address: stephane.lucas@fundp.ac.be (S. Lucas).

0257-8972/$ – see front matter © 2011 Elsevier B.V. All rights reserved.
doi:10.1016/j.surfcoat.2011.04.077

Table 1
Main characteristics and production routes of the Co and Au radioisotopes used in this study.

Radioisotope	Half life (days)	Production route	Main γ-radiations (keV)
^{57}Co	272	1 - ^{59}Co(p,p2n)^{57}Co 2 - decay of ^{57}Ni (produced by ^{59}Co(p,3n)^{57}Ni)	122 and 136
^{58}Co	71	^{59}Co(p,pn)^{58}Co	811
^{195}Au	186	1 - ^{197}Au(p,p2n)^{195}Au 2 - decay of ^{195}Hg (produced by ^{197}Au(p,3n)^{195}Hg)	99
^{196}Au	6	^{197}Au(p,pn)^{196}Au	356 and 333

elements in bimetallic NPs are questionable and change in miscibility may help to design novel alloyed NPs possessing unique properties that may not be obtained as bulk materials.

In order to ensure that NPs, when put in water solution, act as separate entities and do not aggregate together, in-situ post-synthesis functionalization with a Plasma Polymer Allylamine (PPAA) layer was performed. This treatment insures that NPs are monodispersed and stay as such for at least two weeks in the solution [5]. This delay is convenient for appropriate manipulation and measurements of radioactive solutions.

2. Experimental set up

Depositions were performed by high pressure magnetron discharge. Radioactive targetry was elaborated by depositing radioactive metallic disks (0.8 cm diameter, 100 μm thick) on a non-radioactive Au target. The radioisotopes of Co ($^{57/58}$Co) and Au ($^{195/196}$Au) used in this work were produced at the cyclotron of the Joint Research Centre, European Commission (Ispra, Italy). The cyclotron is a Scanditronix MC 40 model (K = 40) able to accelerate 4 different particles (p, d, α and $^{3}He^{2+}$) at variable energies. ^{57}Co and ^{58}Co radioisotopes are simultaneously produced by proton beam bombardment of disks of pure Co. ^{57}Co is produced via the nuclear reactions ^{59}Co(p,p2n)^{57}Co and by decay of ^{57}Ni radioisotope which is activated by the nuclear reaction ^{59}Co(p,3n)^{57}Ni while ^{58}Co is mainly produced by the reaction ^{59}Co(p,pn)^{58}Co. In the case of ^{196}Au and ^{195}Au, they are activated through proton beam bombarding disks of pure Au. ^{195}Au is activated via the reaction ^{197}Au(p,p2n)^{195}Au and by decay of ^{195}Hg which is simultaneously produced through the reaction ^{197}Au(p,3n)^{195}Hg. ^{196}Au is produced via the single nuclear reaction channel ^{197}Au(p,pn)^{196}Au.

These radioisotopes have been chosen for their suitable half life which allow us to perform relatively long term (without significant radioactive decay) experiments of stability of the produced radioactive NPs. They are also chosen for their γ − radiation which can be detected with high precision and accuracy. Table 1 presents the main characteristics of these radioisotopes including the nuclear reactions cyclotron production routes.

In both Co and Au cyclotron irradiations, several disks were prepared and irradiated in a single cyclotron irradiation run of several hours. Considering the optima cross sections of the mentioned nuclear reactions for high radioisotope production yields, proton beam energies of 32 and 30 MeV were used for Co and Au targets respectively. The Co and Au disks respectively were put in an Al capsule which was inserted into a target holder equipped with a water cooling system to avoid over heating of the disks during the cyclotron irradiations. Fig. 1 presents a schematic design of the water cooled target system.

During the irradiations, the beam intensity was monitored via a Faraday cup on which the target was mounted. After the end of each irradiation, several days of radioactive decay were necessary to allow the dose rate to reduce somewhat and allow handling of the activated samples at minimum radiation exposure to the workers. Considering the cross-section and the energy loss, the disks were activated homogeneously all over their thicknesses.

The disks were then shipped to Belgium and inserted into the deposition equipment that is presented in Fig. 2. A turbomolecular pump is used to obtain a base pressure of 10^{-4} Pa. The chamber is equipped with a magnetron sputtering source and a thermal evaporation source. The latter consists of a tantalum evaporation boat source filled with NaCl grain (99.9% purity) and maintained between 2 clamps connected to AC current (i ≅ 80A and V ≅ 3 V). A Quartz Crystal Monitor (QCM) is mounted near the sample on the substrate holder for monitoring the amount of NaCl deposit. The Au

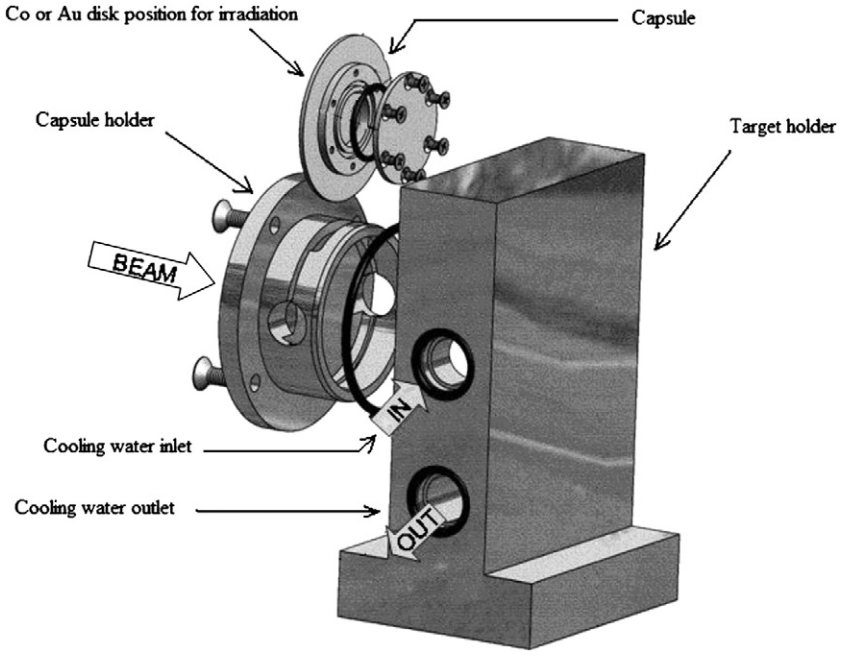

Fig. 1. Schematic design of water cooled target system used to perform disk activation.

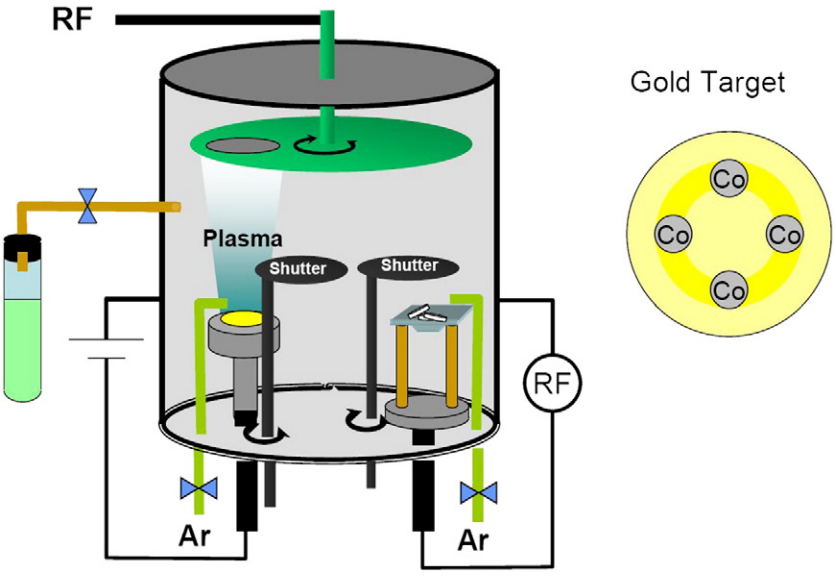

Fig. 2. Schema of the experimental setup and the gold target used to synthesize PPAA-coated Au NPs.

NPs are generated by sputtering with Argon gas a 99.99% gold target (2", 0.0625" thickness) mounted on the magnetron deposition gun and eventually loaded with the radioactive disks placed in the race track. A pressure of 24 Pa and an argon gas flow of 20 SCCM in the vacuum chamber, controlled by a mass flow controller and a VAT adaptive valve were used. The power supply was set at 75 W and the deposition time at 2 s.

Five experiments were performed with different total activities of ^{58}Co: 39, 95, 1200, 2170 and 2890 MBq. A last test of this method was performed with activated gold disks; ^{196}Au (95%) and ^{195}Au (5%) with a total activity of 1390 MBq. Typical concentration of radioactive atom per disk is 1 ppm. Substrates used to collect NaCl and Au NPs are stainless steel disks with a total deposition surface of 61.5 cm². Substrates are mounted in a substrate holder which was electrically isolated from the chamber and connected to a radiofrequency (RF) power supply (13.56 MHz). The distance between the substrate holder and the sputtering or thermal sources is 9.0 cm. Au NPs were post-functionalized with PPAA by injecting allylamine vapor inside the vacuum chamber and by applying a RF power of 10 W to the substrate holder. The monomer allylamine (98%, purchased from Sigma-Aldrich) used for the functionalization of these Au NPs is introduced in a glass vacuum flask connected to the vacuum chamber. A flow control valve is placed between the flask and the chamber in order to maintain a constant pressure of 8 Pa inside the vacuum chamber during the experiment. More details concerning the PPAA coating can be found in previous papers [5,12].

Four different steps are required to produce radioactive NPs suspended in solution. The process starts with a NaCl deposition of 100 nm thick on the substrate by evaporation. This step is followed by the synthesis of radioactive Au NPs by magnetron sputtering. By working at high pressure, free atoms released from the radioactive thin circular films of Co or Au aggregate with the free atoms sputtered from the gold target to form small radioactive NPs in gas phase. Also called cluster beam deposition, it has the advantage to produce non-agglomerated NPs with a narrow size distribution onto any desired substrate as NaCl [5,13]. The sputtering rates under our operating conditions were assessed experimentally with a QCM to 4.8 Å/s for gold and 1.0 Å/s for cobalt, meaning that about five times more gold atoms are sputtered from the target than cobalt atoms. The third step is the functionalization of these Au NPs with Plasma Polymerized Allylamine (PPAA). Surface functionalization with polymeric macromolecules is essential to stabilize these Au NPs in aqueous solution against aggregation [5]. When the synthesis and the functionalization are completed, the last step of production consists of collecting the radioactive Au NPs by dissolving the NaCl in 12 ml of pure water. After ultrasonication for 15 min, the solution becomes red which is the characteristic color of monodispersed small Au NPs in solution.

Activity of substrates and solutions were measured using a CAPINTEC well counter or a High Purity Germanium (HPGe) detector system. Due the low activity of some samples, these measurements were performed under a low surrounding radiation background to ensure high accuracy and sensitivity of measurements (see next section). Sizes, morphologies and dispersion of these radioactive NPs in solution were analyzed by Transmission Electron Microscopy (TEM), by CPS disk centrifuge and by using UV-Visible spectrophotometer.

3. Results and discussion

Three different types of analyses have been used to control the synthesis process by physical vapor deposition as well as the stability of the produced monodispersed radioactive Au NPs. The first one is the characterization of these Au NPs in solution by different methodologies to measure their sizes, their dispersion and their stability in solution. The second analysis concerns the activity measurements. In this section, activities of the samples before and after their transfer in 12 ml of pure water were measured, as well as the activity transfers between target-substrate and substrate solution that confirm that the radioactive atoms are well embedded in the Au NPs.

3.1. Characterization of PPAA-coated Au NPs in solution

For the characterisation of our radioactive Au NPs in solution, samples of AuNPs doped with ^{58}Co or ^{196}Au and functionalized with PPAA were prepared and transferred into 12 ml of pure water. UV-Vis spectrophotometry, CPS measurements, and TEM images provide crucial information on the morphology, the sizes and the stability of these NPs in aqueous solution.

The different solutions were mainly analyzed by CPS disk centrifuge. The mean diameter for Au NPs doped with ^{196}Au is 6 ± 1 nm. With a radius of 5 ± 3 nm, the same mean size is observed for Au NPs mixed with ^{58}Co. The latter is calculated by making the average of values obtained from the five different experiments with initial activities varying between 39 and 2890 MBq on the target

Table 2
Evolution of the maximum absorption (λ_{max}), the peak intensity and the FWHM of plasmon bands obtained with the UV-Vis spectrophotometer for Au NPs doped with ^{58}Co. First measurements of the samples (T_0) were performed just after their production and the second set of data were obtained 2 weeks after their production. The last line of this table also gives the time evolution of their mean diameter resulting from the CPS disk centrifuge.

Transfer [/cm^2]	^{58}Co	^{196}Au
Target – Substrate	5.28×10^{-8}	2.41×10^{-7}
Target – Solution	3.82×10^{-8}	1.97×10^{-7}
Substrate – Solution	72%	82%

before sputtering. Samples of Au NPs doped with ^{58}Co were analyzed a second time, 2 weeks after their production, to see the evolution of their mean size with time. As presented in the last line of Table 2, PPAA-coated Au NPs seem to present a small increase of their mean diameter with time. This is probably due to the presence of free polymers macromolecules in water solution which are adsorbed on the Au NPs after a while. These free polymers macromolecules can originate from depositions of PPAA between the spaced Au NPs on the NaCl layer during the functionalization.

For TEM studies, drops of the different solutions containing Au NPs were placed on 3 mm copper grids covered with carbon films and analyzed by transmission electron microscopy on a Phillips TECNAI-10. For each sample, TEM images show Au NPs with spherical, hexagonal, triangular or square shapes (Fig. 3). Except for some NPs which stack together, the majority of them are well dispersed and relatively uniform in sizes. Diameters observed on the TEM grids have a mean value of 9 ± 2 nm for the experiments with ^{58}Co and 11 ± 3 nm for the experiments with ^{196}Au. They are larger than those obtained with the CPS disk centrifuge. The difference between both methods can be explained by the fact that the density of PPAA-coated Au NPs is difficult to define, and yet this parameter is essential for the diameter measurements with the CPS disk centrifuge.

According to the CPS disk centrifuge and TEM images, the mean sizes of the Au NPs seem smaller than 10 nm. Confirmation was provided by ultraviolet-visible spectrophotometry (Perkin Elmer Lambda 20). Fig. 4 gives an example of surface plasmon absorption spectra for Au NPs doped with ^{58}Co solutions sampled just after the Au NPs synthesis. The same sample was also analyzed 2 weeks later to study the aging of Au NPs production. Measurements concerning the maximum, the intensity and the full width at half maximum (FWHM) for both plasmon peaks are given in Table 2. Just after the Au NPs synthesis, the curve shows a plasmon absorption band with the maximum located around 530 nm. The latter is characteristic of non-

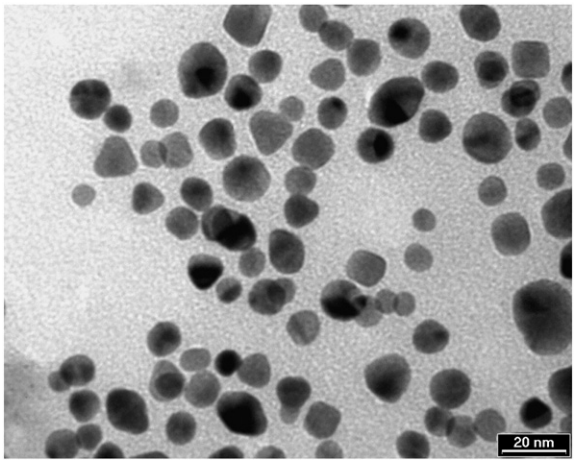

Fig. 3. TEM image of Au NPs mixed with ^{58}Co.

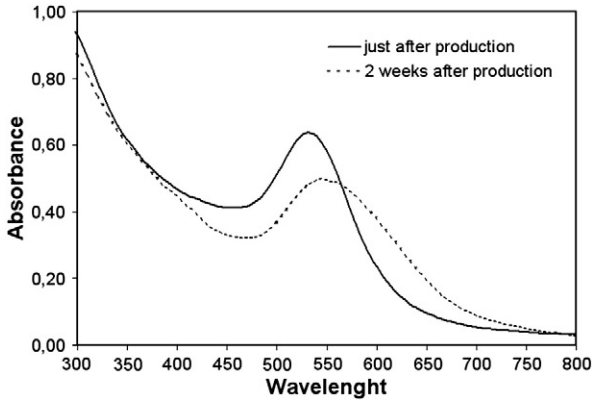

Fig. 4. Surface plasmon absorption spectra of spherical Au NPs doped with ^{58}Co in 12 ml solution. The solid and dotted lines are obtained just after the production and two weeks later, respectively.

agglomerated AuNPs with small particle diameters and is responsible for the red color of the solution [14,15]. A red-shift of the maximum plasmon peak from 530 to 550 nm is observed after two weeks. So, as already mentioned after the CPS measurements, the Au NPs mean size seems to increase slightly with time. The peak intensity also decreases after two weeks, meaning that a part of these Au NPs have aggregated. Finally, the FWHM of the plasmon peak gives an idea of the size distribution range.

3.2. Activity measurements

Activity measurements were performed with a coaxial HPGe detector (Canberra Industries, Inc) with high relative efficiency and high energy resolution (2.3 at 1332 keV). For lower activity measurements, background noise (mainly caused by natural radioactivity and cosmic radiation) has to be minimized. The problem was solved by using a low-level setup for gamma spectroscopy as described in [16]. For higher activity measurements, a lead brick between the sample and the detector was placed to reduce the dead time during data acquisition. Fig. 5 gives an example of γ-ray spectra for ^{196}Au and ^{58}Co obtained when the HPGe is inside (a,c) and outside (b) the lead castle. ^{58}Co presents two mains γ rays at 511.00 KeV and 810.76 KeV. Activities of the samples for Au NPs doped with this radioactive element were estimated from the intensity of the 810.76 KeV γ peak. For ^{196}Au, activities of the substrates and the solutions were determined through its main γ-ray peak at 355.76 keV. The following Eq. (1) allows us to convert the γ peak intensities into activities:

$$A_0 = \frac{I/\tau}{\exp\left[-\mu.x-\lambda.t\right].\varepsilon_D} \quad (1)$$

where I and τ are respectively the net γ peak area in counts and acquisition times. μ (in cm^{-1}) represents the linear attenuation coefficient for a specific material. μ is used when a lead brick is placed between the detector and the samples to limit the acquisition dead time. Its value was determined by multiplying the photon mass attenuation coefficient given on the NIST site (http://physics.nist.gov/PhysRefData/XrayMassCoef/tab3.html) with the absorber mass density. x (in cm) represents the thickness of the lead brick. λ (in days^{-1}) is the decay constant for ^{58}Co or ^{196}Au and t (in days) is the elapsed time between the production of radioactive Au NPs and the activity measurements by the HPGe. Finally, ε_D determines the efficiency of the detector which depends on the detector geometry and, on the distance between the sample and the germanium crystal. Efficiency of the detector was evaluated by means of Monte Carlo simulation using the software MCNPX 2.5.0 [17,18]. For the stainless steel substrate, the

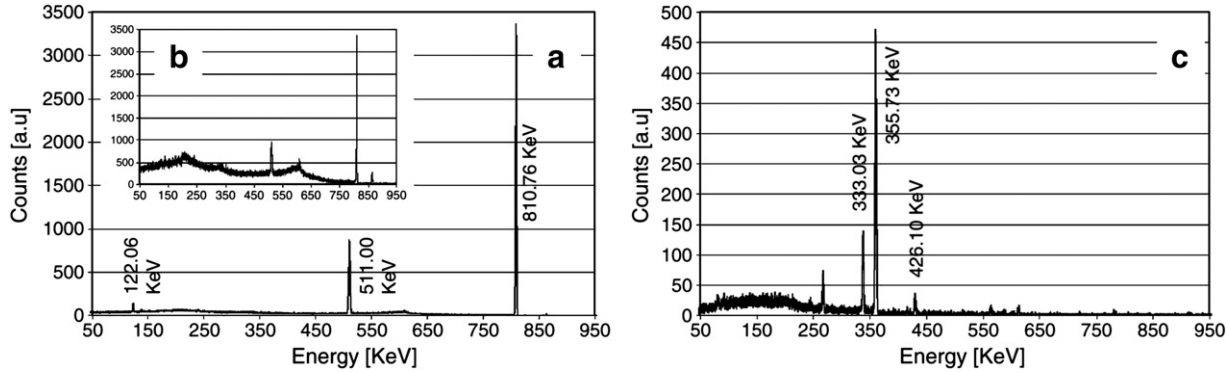

Fig. 5. γ-ray spectra for ^{58}Co measured with the HPGe detector inside (a) and outside (b) the lead castle. On the second spectra, background has totally disappeared. (c) γ-ray spectra for ^{196}Au.

photon source is described by a circular surface with the same diameter as the one used for the deposition of radioactive Au NPs. For the radioactive Au NP solutions, the photon source is described by a cylindrical volume with a height of 9.2 cm and a diameter of 1.6 cm. The efficiency is calculated directly from the "pulse height tally" (Tally F8) which gives the distribution of the deposited energy in a detector. Simulations are performed in mode p–e (transportation of photons and electrons) for at least 10^7 source particles providing a statistical uncertainty on the full-energy peak of less than 0.5%. Activities of the Au NP solutions were systematically calculated from a CAPINTEC γ well and are in good agreement with those resulting from the HPGe detector. This result allows us to verify that the detector efficiency determined with the Monte Carlo code and the other parameters introduced in Eq. (1) to calculate the activities are correct.

Fig. 6 presents activities of the substrates, in kBq/cm², as a function of the five different initial activities (39, 95, 1200, 2170 and 2890 MBq). As shown in Fig. 6, activities deposited on the substrate increases linearly with the initial activities loaded on the gold target before sputtering. Activity transfer, by cm² of substrate, for gold nanoparticles doped with ^{58}Co and ^{196}Au are given in Table 3. Values are determined for activity transfer between the target and the substrate before dissolution of the Au NPs and between the target and the solution. As we can see in this table, activity transfer between thin disks of radioactive gold and substrate are larger by a factor of 4.6 than the one between thin circular cobalt films and substrate. This value is identical to the one determined in the experimental part between the sputtering rate for cobalt and gold. By knowing the sputtering rate of any material used for the thin circular films, we are now able to define the activity transfer by simply dividing 2.41×10^{-7} by the sputtering rate of this material. This transfer rate can be considered as low. But two major reasons account for that: 1- only surface atoms are sputtered from the disks while the transfer rate is being calculated by taking into account the overall activity of the disks. 2- Backscattering of the sputtered species by the gas phase is significant as it was revealed by measuring the activity on the various parts surrounding the magnetron gun.

Table 3 gives also the percentage of activity transfers between the substrate and the solution obtained by making the ratio of both activity transfers target-substrate and target-solution. Results are higher than 70% showing that the method used to collect the PPAA-coated Au NPs is practical. The balance was found to remain on the substrate holder.

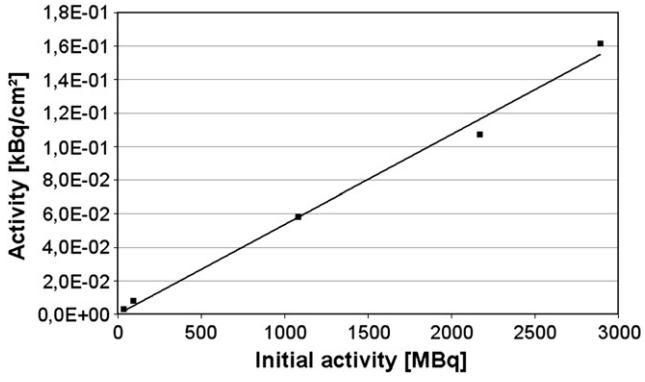

Fig. 6. Activity samples versus initial activity put down on the gold cathode before sputtering.

Table 3
Activity transfers by cm² between target and substrate and between target and solution.

	T_0	2 weeks
λ_{max} [nm]	530	550
Peak intensity	0.6	0.5
FWHM	77	94
CPS diameter [nm]	5 ± 3	7 ± 4

3.3. Centrifugation analyses

The objective of this paragraph is to verify that radioactive atoms are well embedded in the Au NPs. Centrifugation of solutions was performed and the supernatant was separated from the pellets constituting the aggregated Au NPs. If a large part of the activity is found in the supernatant, we can conclude that radioactive atoms are largely present in the water under an ionic form or as very small NPs.

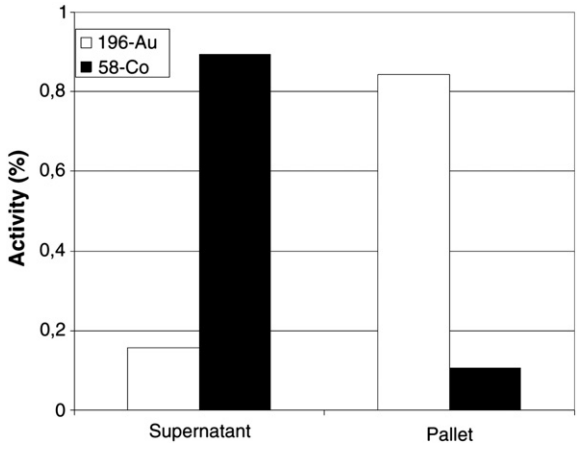

Fig. 7. Activity of the supernatant and the pellet after solution centrifugation of Au NPs synthesized with ^{58}Co or ^{196}Au.

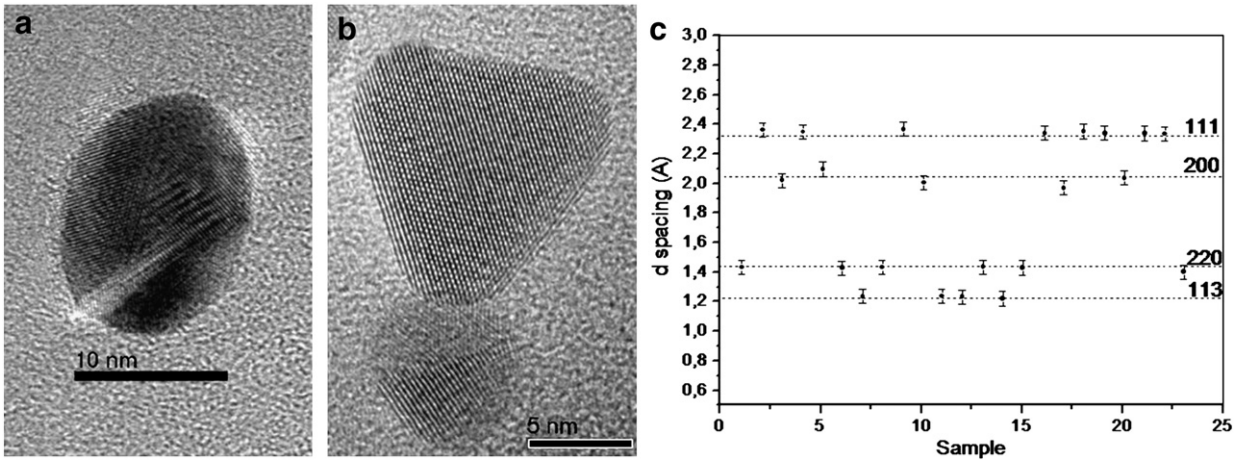

Fig. 8. High-resolution TEM images of a hexagonal (a) and a triangular (b) PPAA-coated Au NPs doped with Co. (c) corresponds to d spacing of numerous Au NPs as observed in Fig. 3.

Inversely, the radioactive and the corresponding cold atoms are alloyed with Au if the pellet is more radioactive than the supernatant.

The experiment consists of taking 1 ml of the different solutions containing Au NPs mixed with ^{58}Co or ^{196}Au. Solutions are placed in different Eppendorf vials and centrifuged for 2 h at 60,000 rpm. Before centrifugation, activities and gold concentrations of these solutions were determined by using the HPGe detector. After centrifugation, both the supernatant and the gold pellet at the bottom were collected in two new flasks to analyze their activity with the HPGe detector and their gold concentration by Atomic Absorption Spectroscopy Analysis.

For all solutions, the supernatant was slightly pink which means that a small amount of very small Au NPs is still present in the liquid after centrifugation. However, a strong difference appears about the activities between Au NPs mixed with ^{58}Co and Au NPs mixed with ^{196}Au. Indeed, for experiments with ^{58}Co, the percentage of activities observed after centrifugation in the pellet and the supernatant are clearly opposed to the one of ^{196}Au experiments as described in Fig. 7. This result indicates that no or very few radioactive atoms are incorporated into the Au NPs. Inversely, the ^{196}Au atoms are doping the non-radioactive NPs since after centrifugation, 83% of the total activity of the solutions is found in the pellet. The results are in accordance with the Au–Co phase diagram [7]. Indeed, four equilibrium phases are found: liquid, Au fcc solid solution with a maximum solubility of 23% of Co at 996.5 °C, a high T° Co fcc solid solution with a maximum solubility of 2.5 at.% Au, and a low temperature cph solid-solution with a limited Au solubility of 0.05%.

According to this phase diagram, no phase made out of Au with a small amount of Co can be observed below 422 °C. Nevertheless, one can ask: what about the 15% of the ^{58}Co found in the pellet? Taking into account the sputter yield, the ratio Co/^{58}Co in the radioactive disks, the Au/Co atomic ratio in the NP correspond to 20–50% depending on the nanoparticle size. This large amount of Co should induce a distortion of the bimetallic lattice parameter when compared to Au. In order to verify that, a sample was investigated by HRTEM (Cs corrected TITAN) operated at 200 keV. It has to be noted that no activity was detectable in the TEM grid. Fig. 8 (a) and (b) exhibit the lattice fringes of spherical and triangular shapes indicating the crystalline nature of all these Au NPs [19]. The structure of the non spherical shaped particles (see Fig. 8(b)) is always seen to be monocrystalline, whereas the other more spherical particles are mostly polycrystalline (see Fig. 8(a)). Interplanar spacing of several particles as measured by taking the Fast Fourier Transform of HRTEM images is presented in Fig. 8(c). As we can see the spacing corresponds strictly to the one of Au. No lattice distortions are observed. Therefore, one can conclude that neither metastable nor alloyed Au/Co phases were formed. Co atoms are probably embedded within alylamine that was deposited on NaCl.

4. Conclusion

In this paper, we describe an approach using physical vapor deposition technology to produce Au NPs potentially doped with radioactive atoms and functionalized with PPAA. NPs are synthesized by magnetron sputtering at high pressure and radioactive atoms are loaded on the magnetron cathode prior to sputtering. The Au NPs are then transferred into pure water and the solution is stable for more than a week.

Two types of radioactive atoms were considered. The first one is ^{58}Co, the second one is ^{196}Au. It was found that Co is not soluble in the Au/Co NPs, and only radioactive ^{196}Au NPs could be produced. TEM investigations have showed that NPs have a mean diameter varying between 5 and 10 nm and that they are well dispersed in water solution. These observations were confirmed by UV-Vis spectroscopy and CPS disk centrifuge analyses.

Activity measurements also have shown that the transfer of activity is very low and does not depend on the initial activity loaded on the cathode before the sputtering. Moreover, activity transfer for different type of radioactive atoms can be foreseen according to the sputtering rate of the radioactive atoms.

Acknowledgments

This research (Targan Project) was supported by the Walloon Region (Belgium). Olivier Feron is senior research associate of FNRS (Fonds National de la Recherche Scientifique, Belgium). The authors acknowledge financial support from the European Union under the Framework 6 program under a contract for an Integrated Infrastructure Initiative. Reference 026019 ESTEEM.

References

[1] A. Bapat, C. Anderson, C.R. Perrey, C.B. Carter, S.A. Campbell, U. Kortshagen, Plasma Phys. Control. Fusion 46 (2004) B97.
[2] Y. Qiang, J. Antony, A. Sharma, J. Nutting, D. Sikes, D. Meyer, J. Nanopart. Res. 8 (2006) 489.
[3] G. Schultes, M. Schmidt, M. Truar, D. Goettel, O. Freitag-Weber, U. Werner, Thin Solid Films 515 (2007) 7790.
[4] I. Shyjumon, M. Gopinadhan, O. Ivanova, M. Quaasz, H. Wulff, C.A. Helm, R. Hippler, Eur. Phys. J. D 37 (2006) 409.
[5] N. Moreau, C. Michiels, B. Masereel, O. Feron, B. Gallez, T.V. Borght, S. Lucas, Plasma Proc. Polym. 6 (2009) S888.
[6] H. Haberland, M. Mall, M. Moseler, Y. Qian, T. Reiners, Y. Thurner, J. Vac. Sci. Tech. A 12 (1994) 2925.

[7] H. Okamoto, T.B. Massalski, H. Hasebe, T. Nishizawa, Bull. Alloy Phase Diagrams 6 (1985) 449.
[8] J. Tersoff, Appl. Phys. Lett. 83 (2003) 353.
[9] G.F. Wang, M.A. Van Hove, P.N. Ross, M.I. Baskes, J. Chem. Phys. 122 (2005).
[10] D.S. Mainardi, P.B. Balbuena, Langmuir 17 (2001) 2047.
[11] F. Lequien, J. Creuze, F. Berthier, B. Legrand, Faraday Discuss. 138 (2008) 105.
[12] S. Lucas, G. Genard, C. Michiels, B. Masereel, O. Feron, B. Gallez, T.V. Borght, N. Moreau, Nucl. Instrum. Methods Phys. Res. Sect. B 266 (2008) 2494.
[13] L. Dreesen, F. Cecchet, S. Lucas, Plasma Proc. Polym. 6 (2009) S849.
[14] F.W. Vance, B.I. Lemon, J.T. Hupp, J. Phys. Chem. B 102 (1998) 10091.
[15] W. Cai, T. Gao, H. Hong, J. Sun, Nanotechnol. Sci. Appl. 1 (2008) 17.
[16] G. Genard, V.E. Nuttens, V. Bouchat, G. Terwagne, Nucl. Instrum. Methods Phys. Res. Sect. B 268 (2010) 1523.
[17] L.E. Waters, MCNPX User's Manual Version 2.4.0, Los Alamos National Laboratory Report, LA-CP-02-408, 2002.
[18] L.E. Waters, MCNPX Version 2.5.e, Los Alamos National Laboratory Report, LA-UR-04-0569, 2004.
[19] H. Nabika, M. Mizuhata, A. Kajinami, S. Deki, K. Akamatsu, J. Electroanal. Chem. 559 (2003) 99.